Physica D 456 (2023) 133936

Contents lists available at ScienceDirect

Physica D

journal homepage: www.elsevier.com/locate/physd

Segregation and domain formation in non-local multi-species aggregation equations

Karl Glasner

Department of Mathematics, University of Arizona, Tucson, AZ 85721, USA

ARTICLE INFO

Communicated by T. Wanner

Keywords:
Aggregation equations
Interacting particle systems
Phase segregation

ABSTRACT

A system of aggregation equations describing nonlocal interaction of two species is studied. When interspecies repulsive forces dominate intra-species repulsion, phase segregation may occur. This leads to the formation of distinct phase domains, separated by moving interfaces.

The one dimensional interface problem is formulated variationally, and conditions for existence and nonexistence are established. The singular limit of large and short-ranged repulsion in two dimensions is then considered, leading to a two-phase free boundary problem describing the evolution of phase interfaces. Long term dynamics are investigated computationally, demonstrating coarsening phenomenon quantitatively different from classical models of phase separation. Finally, the interplay between long-range interspecies attraction and interfacial energy is illustrated, leading to pattern formation.

This paper considers the dynamics of interacting populations, described by coupled aggregation equations for the evolution of densities $\rho_{1,2}$,

$$\frac{\partial \rho_1}{\partial t} = \nabla\cdot(\rho_1 \nabla[K_{11} * \rho_1 + K_{12} * \rho_2]), \tag{1}$$

$$\frac{\partial \rho_2}{\partial t} = \nabla\cdot(\rho_2 \nabla[K_{22} * \rho_2 + K_{12} * \rho_1]). \tag{2}$$

Convolution is defined as $K * u = \int_\Omega K(x-y)u(y)dy$, where Ω is the spatial domain. It will be assumed that Ω is bounded, and that no-flux boundary conditions

$$\nabla[K_{11} * \rho_1 + K_{12} * \rho_2]\cdot \boldsymbol{n} = 0, \quad \nabla[K_{22} * \rho_2 + K_{12} * \rho_1]\cdot \boldsymbol{n} = 0, \tag{3}$$

(where $\boldsymbol{n}$ is the outward normal to the boundary) apply on $\partial\Omega$. Self-interactions are described by the potentials K_{11}, K_{22}, whereas the cross-interaction is specified by K_{12}.

Eqs. (1)–(2) arise as the large number limit of the interacting particle system

$$\begin{aligned} \dot{X}_i &= -\sum_{j=1, j\neq i}^{N_y} \nabla K_{11}(X_i - X_j) + \nabla K_{12}(X_i - Y_j), \\ \dot{Y}_i &= -\sum_{j=1, j\neq i}^{N_x} \nabla K_{22}(Y_i - Y_j) + \nabla K_{12}(Y_i - X_j), \end{aligned} \tag{4}$$

where X_i, Y_i represent positions of particles of species 1 and 2, respectively. Alternatively, the evolution Eqs. (1)–(2) may be regarded as a (Wasserstein-type) gradient flow of the energy functional

$$E = \int_\Omega \frac{1}{2}\rho_1 K_{11} * \rho_1 + \frac{1}{2}\rho_2 K_{22} * \rho_2 + \rho_1 K_{12} * \rho_2 \, dx. \tag{5}$$

Single-species versions of (1)–(2) have been well-studied. Such models arise from a variety of sources, including biological and social phenomenon [1–3]. In this case, there has been a thorough investigation of mathematical well-posedness [4–6]. Equilibrium behavior, such as the formation of swarms and patterned states, has also received significant attention [3,7–10]. Additionally, there have been explorations of dynamic phenomenon (e.g. [11,12]).

In contrast, less is known theoretically about multi-species systems like the one studied here. Models of this form, however, are widespread. Some examples include ecological competition and interaction [13], materials science [14], crowd dynamics [15], opinion dynamics [16, 17], and economic and social segregation [18].

Some fundamental mathematical results have been obtained for the system (1)–(2). Existence of measure-valued solutions was demonstrated in [19]. This was later extended to the case where diffusion was added [20]. There are also a few studies of equilibrium behavior and pattern formation, generally for systems with specific potentials [21–23].

This paper's main interest is in the question of segregation of the two populations into spatially distinct domains. In the circumstance where the potentials are repulsive, the last term in (5) penalizes mixing of the two species, whereas the first two terms favor spreading. Provided the former effect outweighs the latter, densities will evolve to

E-mail address: kglasner@math.arizona.edu.

https://doi.org/10.1016/j.physd.2023.133936
Received 19 June 2023; Received in revised form 5 September 2023; Accepted 25 September 2023
Available online 4 October 2023

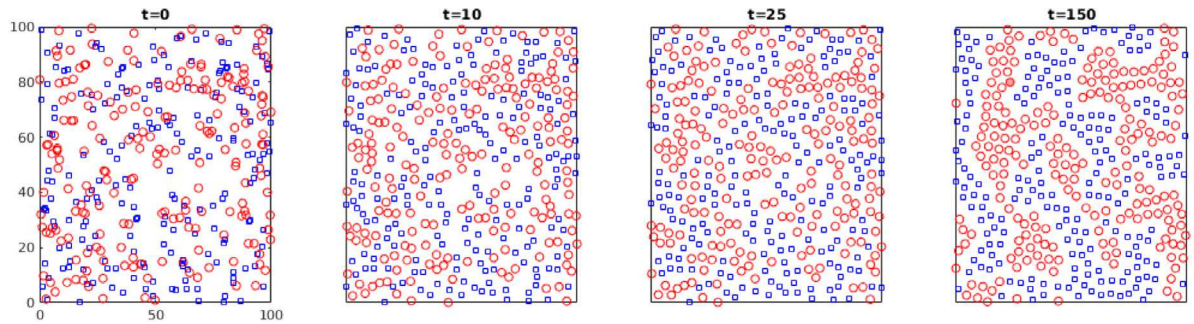

Fig. 1. Simulations of (4) where $N_x = N_y = 200$. The model details are provided in Section 4.1.

form spatial domains characterized by a preponderance of one species. Fig. 1 illustrates this phenomenon for the interacting particle model (4).

The existence of segregated steady states was rigorously verified in [24] for the case where a small diffusion term was added to (1)–(2). The range of parameters for specific interaction potentials which induces phase separation was computed in [25]. Variants of the two species interaction model have also been studied, such as a mean field model of segregation [26], and a constant density version of the underlying variational problem for steady states [27].

Theoretical aspects of phase segregation in the setting of materials science have been well-studied, largely in the context of the celebrated Cahn–Hilliard equation [28]. Nonlocal versions of the Cahn–Hilliard equation have also been derived and analyzed [29,30]. In both the local and nonlocal cases, phase separation results solely from the pointwise (thermodynamic) potential. In contrast, here phase separation is entirely a consequence of nonlocal interactions. Nevertheless, there are some parallels between the two modeling frameworks which are discussed below.

This paper is organized as follows. The primary assumptions of the model and basic results are provided in Section 1. Section 2 studies the one-dimensional interface problem and establishes conditions for segregation to occur. Section 3 considers the singular limit where interaction distances are small. This is done by a multiscale analysis which produces a free boundary problem describing the evolution of domain interfaces. In Section 4, numerical simulations of both the particle and continuum models are used to investigate large-scale coarsening effects. Finally, the role of long-range attractive forces is considered in Section 5.

1. Preliminaries

Most of the paper is dedicated to interactions which are only repulsive. The potentials $K_{11}, K_{22}, K_{12} \in L^1(\mathbb{R}^n) \cap C_2(\mathbb{R}^n)$ are taken to be radially symmetric, positive and strictly decreasing for $|x| > 0$, representing isotropic repulsion. Additionally, potentials are assumed to decay as $K = O(e^{-\alpha|x|}), x \to \infty$ for some $\alpha > 0$. This has the effect of localizing interactions near interfaces. In Section 5, we allow for potentials to have a long-range attractive component as well.

It will generally be assumed that $\rho_{1,2}$ are in $L^1_{loc}(\Omega)$, rather than just probability measures as in [19]. An exception to this is noted for boundary layers in Section 3.3, wherein mass may concentrate on $\partial\Omega$.

1.1. Stability of a homogeneous state

We first consider the stability of a uniform density $(\rho_1(x), \rho_2(x)) \equiv (\overline{\rho}_1, \overline{\rho}_2)$ for $x \in \mathbb{R}^n$. There are two qualitatively different cases, where either one species is zero, or neither is.

In the situation where both $\overline{\rho}_1 > 0$ and $\overline{\rho}_2 > 0$, perturbations evolve by linearization of (1)–(2)

$$\frac{\partial \rho_1}{\partial t} = \nabla\cdot(\overline{\rho_1}\nabla[K_{11} * \rho_1 + K_{12} * \rho_2]), \tag{6}$$

$$\frac{\partial \rho_2}{\partial t} = \nabla\cdot(\overline{\rho_2}\nabla[K_{22} * \rho_2 + K_{12} * \rho_1]). \tag{7}$$

Seeking modes of the form $(\rho_1(x), \rho_2(x)) = \exp(\sigma t + ik\cdot x)(A_1, A_2)$ leads the fact that σ is an eigenvalue of

$$-|k|^2 \begin{pmatrix} \overline{\rho_1}\hat{K}_{11}(k) & \overline{\rho_1}\hat{K}_{12}(k) \\ \overline{\rho_2}\hat{K}_{12}(k) & \overline{\rho_2}\hat{K}_{22}(k) \end{pmatrix}$$

where $\hat{f}$ denotes the usual Fourier transform. Under the assumptions given above for purely repulsive interactions, it is easy to show that $\hat{K}_{ij} > 0$ for $i, j = 1, 2$. Positive eigenvalues, and therefore instability, are only possible when the determinant is negative,

$$\hat{K}_{12}^2 > \hat{K}_{11}\hat{K}_{22} \quad \text{for some } k. \tag{8}$$

In other words, sufficient cross-species repulsion will induce instability.

On the other hand, for the case $\overline{\rho}_1 = 0$ (or vice-versa), perturbations of ρ_1 must be positive, but these would not preserve mass. In this case, the linearized evolution involves only ρ_2 and is always stable. The picture which emerges is a degenerate version of the classical description of spinodal decomposition, wherein mixtures are unstable over a range of composition ratios, but are stable when one species in a homogeneous mixture is highly dilute [28].

2. Domain interfaces

We first consider one-dimensional equilibria which describe the interface between bulk domains. Taking $\Omega = \mathbb{R}$, steady states of (1)–(2) satisfy

$$K_{11} * \rho_1 + K_{12} * \rho_2 = \overline{\mu}_1, \quad x \in \text{spt}\rho_1, \tag{9}$$

$$K_{22} * \rho_2 + K_{12} * \rho_1 = \overline{\mu}_2, \quad x \in \text{spt}\rho_2, \tag{10}$$

where $\overline{\mu}_{1,2}$ are constants to be determined. Solutions of this system with finite mass have been studied previously [23]. In contrast, we seek a solution describing a transition from one single-species domain to another by imposing the conditions

$$\lim_{x\to-\infty}(\rho_1, \rho_2) = (0, \rho_{2\infty}), \quad \lim_{x\to\infty}(\rho_1, \rho_2) = (\rho_{1\infty}, 0). \tag{11}$$

Energy considerations will show that the far field densities $\rho_{1\infty}, \rho_{2\infty}$ cannot be prescribed independently.

The focus of this section is to look for solutions of (9)–(11) which represent an isolated domain interface. A *segregated* solution to (9)–(10) is one where the support of ρ_1 has a lower bound, and the support of ρ_2 has an upper bound. Conditions for the existence or nonexistence of segregated domain interface solutions are explored below.

2.1. Energy balance

Taking $x \to \pm\infty$ in (9) and (10), we see that

$$\overline{\mu}_1 = M^0_{11}\rho_{1\infty}, \quad \overline{\mu}_2 = M^0_{22}\rho_{2\infty}, \quad M^0_{ij} \equiv \int K_{ij}(x)dx, \tag{12}$$

(throughout, integration is over $\mathbb{R}$ unless noted). Multiplying (9) by ρ_1' and (10) by ρ_2' (which exist at least as distributions when $\rho_{1,2} \in L^1_{loc}$), integrating from $-\infty$ to ∞, and summing produces

$$\int \rho_1' K_{11} * \rho_1 + \rho_2' K_{22} * \rho_2 + \rho_1' K_{12} * \rho_2 + \rho_2' K_{12} * \rho_1 dx = \int \overline{\mu}_1 \rho_1' + \overline{\mu}_2 \rho_2'. \tag{13}$$

For $\phi(x), \psi(x) \in L^1_{loc}$, the identity

$$\begin{aligned}\iint K(x-y)\phi'(x)\psi(y)dx\,dy &= -\iint K'(x-y)\phi(x)\psi(y)dx\,dy \\ &= -\iint K(x-y)\phi(x)\psi'(y)dx\,dy,\end{aligned} \tag{14}$$

can be used to show that the integral on the left hand side in (13) is zero. It follows that $\rho_{1\infty}$ and $\rho_{2\infty}$ are related by

$$\frac{1}{2}M^0_{11}\rho^2_{1\infty} = \frac{1}{2}M^0_{22}\rho^2_{2\infty} \equiv e_0. \tag{15}$$

This can be interpreted as a result of energy balance for $x \to \pm\infty$; if this was not the case there would be incentive for the interface to move left or right.

2.2. Variational formulation

Problem (9)–(10) can be associated with an unconstrained minimization problem involving the energy functional

$$\begin{aligned}E_I(\rho_1,\rho_2) &= \int \frac{1}{2}\rho_1 K_{11} * \rho_1 + \frac{1}{2}\rho_2 K_{22} * \rho_2 + \rho_1 K_{12} * \rho_2 \\ &\quad - \overline{\mu}_1\rho_1 - \overline{\mu}_2\rho_2 + e_0\,dx \qquad (16)\\ &= \int \frac{1}{2}(\rho_1-\rho_{1\infty})K_{11} * (\rho_1-\rho_{1\infty}) + \frac{1}{2}(\rho_2-\rho_{2\infty})K_{22} * (\rho_2-\rho_{2\infty}) \\ &\quad + \rho_1 K_{12} * \rho_2 - e_0\,dx. \qquad (17)\end{aligned}$$

where e_0 is defined in (15). This is defined over admissible states, specifically $\rho_{1,2} \in L^1_{loc}(\mathbb{R})$ satisfying (11). Divergence of the integral as $x \to \pm\infty$ is avoided by including the common energy density e_0 in the integrand. It is a straightforward application of the calculus of variations to show that a minimizer of (16) satisfies (9)–(10).

2.3. Nonexistence

In the case where the repulsive interaction between species is not sufficiently strong, mixing should occur and interfaces should not form. This can be quantified in the following result.

Proposition 1. *Suppose that $(M^0_{12})^2 < M^0_{11}M^0_{22}$. Then (16) has no segregated local minimizers.*

Proof. Suppose to the contrary that (ρ_1,ρ_2) is a local minimizer satisfying (11). For any $\epsilon > 0$, let x_ϵ be large enough so that $\rho_1 < \rho_{1\infty}+\epsilon$ and $\rho_2 = 0$ when $x > x_\epsilon$. Let $\phi(x) = \epsilon\phi_0(x-x_\epsilon)$ where $\phi \geq 0$, spt$\phi \in (x_\epsilon,\infty)$ and $\int \phi_0(x)dx = 1$.

Consider now the effect of $\phi(x)$ as a perturbation of ρ_2. Using (12), the change in energy is

$$\begin{aligned}\Delta E &= E_I(\rho_1,\rho_2+\phi) - E_I(\rho_1,\rho_2) \qquad (18)\\ &= \int_{x_\epsilon}^{\infty} \phi K_{12} * \rho_1 - \overline{\mu}_2\phi + \frac{1}{2}\phi K_{22} * \phi\,dx \qquad (19)\\ &\leq \epsilon\int_{x_\epsilon}^{\infty} \phi_0(x-x_\epsilon)(K_{12} * \rho_{1\infty} - M_{22}\rho_{2\infty})\,dx \\ &\quad + \frac{\epsilon^2}{2}\int \phi_0 K_{22} * \phi_0\,dx + \epsilon^2 M_{12}. \qquad (20)\end{aligned}$$

Using (15), this can be written

$$\Delta E \leq \epsilon\rho_{2\infty}\sqrt{M_{22}/M_{11}}\left(M_{12} - \sqrt{M_{11}M_{22}}\right) + O(\epsilon^2). \tag{21}$$

For small enough ϵ, $\Delta E < 0$, so that (ρ_1,ρ_2) cannot be a minimizer. □

2.4. A lower bound on the energy

Clearly a necessary condition for the existence of a global minimizer is a lower bound on (16). The converse of the preceding result is not always true however: even if $(M^0_{12})^2 > M^0_{11}M^0_{22}$, potentials may be specified so as to introduce instabilities at finite wavelengths, and the energy can remain unbounded. A lower bound can be obtained, however, with a stronger condition.

We define the *critical potential* K^* to be the inverse Fourier transform of $\sqrt{\hat{K}_{11}\hat{K}_{22}}$. It is easy to see that K^* is even and bounded. The following proposition guarantees that if interspecies repulsion given by K_{12} is sufficiently large, then a lower bound for (18) is assured.

Proposition 2. *Suppose that $K_{12}(x) > K^*(x)$ for all x. Then there exists a constant C so that $E_I(\rho_1,\rho_2) > C$ for every admissible pair (ρ_1,ρ_2).*

Proof. Let

$$\sigma_1 = \begin{cases}\rho_{1\infty} & x > 0,\\ 0 & x < 0,\end{cases} \qquad \sigma_2 = \begin{cases}\rho_{2\infty} & x < 0,\\ 0 & x > 0.\end{cases} \tag{22}$$

and let $\phi_j = \rho_j - \sigma_j$ for $j = 1,2$. Using this definition and (12),

$$\begin{aligned}E_I(\rho_1,\rho_2) = \int &\frac{1}{2}\phi_1 K_{11} * \phi_1 + \frac{1}{2}\phi_2 K_{22} * \phi_2 + \phi_1 K_{12} * \phi_2 \\ &+ \phi_1 K_{11} * (\sigma_1 - \rho_{1\infty}) \\ &+ \phi_2 K_{22} * (\sigma_2 - \rho_{2\infty}) + \phi_1 K_{12} * \sigma_2 + \phi_2 K_{12} * \sigma_1 dx + C_1,\end{aligned} \tag{23}$$

where

$$C_1 = \int \frac{1}{2}\sigma_1 K_{11} * \sigma_1 + \frac{1}{2}\sigma_2 K_{22} * \sigma_2 + \sigma_1 K_{12} * \sigma_2 - e_0 = \int \sigma_1 K_{12} * \sigma_2, \tag{24}$$

since $e_0 = \frac{1}{2}\sigma_1\overline{\mu}_1 + \frac{1}{2}\sigma_2\overline{\mu}_2$. Notice that all kernels $K_{ij}(x-y)$ are integrable on $Q_2 \cup Q_4$, where $Q_1,\ldots,Q_4$ are the conventional Cartesian quadrants. Therefore the integral defining C_1 is bounded, and additionally any contribution from these quadrants can be selectively removed or added without altering the boundedness property.

Now write $E_I = I_1 + I_2 + I_3 + C_1$ where

$$I_1 = \int_{\mathbb{R}^2} \frac{1}{2}K_{11}(x-y)\phi_1(x)\phi_1(y) + \frac{1}{2}K_{22}(x-y)\phi_2(x)\phi_2(y)\,dxdy, \tag{25}$$

$$\begin{aligned}I_2 = \int_{Q_1\cup Q_4} &K_{12}(x-y)\phi_2(x)(\phi_1(y)+\rho_{1\infty}) \\ &- K_{22}(x-y)\phi_2(x)\rho_{2\infty}\,dxdy + C_2,\end{aligned} \tag{26}$$

$$\begin{aligned}I_3 = \int_{Q_2\cup Q_3} &K_{12}(x-y)\phi_1(x)(\phi_2(y)+\rho_{2\infty}) \\ &- K_{22}(x-y)\phi_1(x)\rho_{1\infty}\,dxdy + C_3,\end{aligned} \tag{27}$$

where C_2, C_3 account for bounded contributions from Q_2 and Q_4. Using $K_{12} > K^*$ we have

$$\begin{aligned}&\int_{Q_1\cup Q_4} K_{12}(x-y)\phi_2(x)(\phi_1(y)+\sigma_1)\,dxdy \\ &\geq \int_{Q_1\cup Q_4} K^*(x-y)\phi_2(x)\phi_1(y)\,dxdy \\ &\quad + \int_{Q_1\cup Q_4} K^*(x-y)\phi_2(x)\rho_{1\infty}\,dxdy.\end{aligned} \tag{28}$$

Since $\int K^*(x)dx = \hat{K}^*(0) = \sqrt{\hat{K}_1(0)\hat{K}_2(0)} = M^0_{22}\rho_{2\infty}/\rho_{1\infty}$ by virtue of (15), the last integral in (28) cancels the negative integral contribution involving $K_{22}(x-y)$ in (26). A similar argument can be applied to I_3, so that

$$I_2 + I_3 \geq \int_{\mathbb{R}^2} K^*(x-y)\phi_1(x)\phi_2(y)\,dxdy + C_4, \tag{29}$$

where C_4 accounts for all the bounded contributions from integrals on Q_2, Q_4.

Finally, by the convolution formula and Plancherel theorem,

$$\begin{aligned} E_I - C_1 - C_4 \geq & \int_{\mathbb{R}} \frac{1}{2}\hat{K}_{11}(k)\hat{\phi}_1(k)^2 + \frac{1}{2}\hat{K}_{22}(k)\hat{\phi}_2(k)^2 \\ & + \sqrt{\hat{K}_{11}(k)\hat{K}_{22}(k)}\hat{\phi}_1(k)\hat{\phi}_2(k)dk \qquad \square \\ = & \frac{1}{2}\int_{\mathbb{R}}\left(\sqrt{\hat{K}_{11}(k)}\hat{\phi}_1(k) + \sqrt{\hat{K}_{22}(k)}\hat{\phi}_2(k)\right)^2 dxdy \geq 0. \end{aligned} \tag{30}$$

2.5. An exact interface profile solution

Exact solutions for nonlocal equations are generally unobtainable, except when the interaction kernels have special properties. To illustrate an explicit segregated solution of (9)–(10), we consider so-called Morse potentials

$$K_{ij}(x) = a_{ij}\exp(-|x|/\ell_{ij}), \quad i,j \in \{1,2\}. \tag{31}$$

Observe that these are scaled Green's functions satisfying

$$\left(-d^2/dx^2 + \ell_{ij}^{-2}\right)K_{ij}(x) = a_{ij}/(2\ell_{ij})\delta(x). \tag{32}$$

Applying operators $(-d^2/dx^2 + \ell_{11}^{-2})(-d^2/dx^2 + \ell_{12}^{-2})$ and $(-d^2/dx^2 + \ell_{22}^{-2})(-d^2/dx^2 + \ell_{12}^{-2})$ to (9) and (10), respectively, produces a system of the form

$$a_{11}/(2\ell_{11})(-d^2/dx^2 + \ell_{12}^{-2})\rho_1 + a_{12}/(2\ell_{12})(-d^2/dx^2 + \ell_{11}^{-2})\ \rho_2 = C_1, \quad x \in \mathrm{spt}\rho_1, \tag{33}$$

$$a_{12}/(2\ell_{12})(-d^2/dx^2 + \ell_{22}^{-2})\rho_1 + a_{22}/(2\ell_{22})(-d^2/dx^2 + \ell_{12}^{-2})\ \rho_2 = C_2, \quad x \in \mathrm{spt}\rho_2, \tag{34}$$

where C_1, C_2 are constants. We consider only the case where the supports of ρ_1, ρ_2 are disjoint, so that with suitable translation we can write $\mathrm{spt}\rho_1 = (x_1, \infty)$ and $\mathrm{spt}\rho_2 = (-\infty, -x_1)$. In this case, Eqs. (33) and (34) decouple, and the general solutions are

$$\rho_1 = \rho_{1\infty} - A_1\exp(-x/\ell_{12}), \quad x > x_1, \tag{35}$$

$$\rho_2 = \rho_{2\infty} - A_2\exp(-x/\ell_{12}), \quad x < -x_1. \tag{36}$$

The unknowns A_1, A_2, x_1 can be determined by substitution into the integral form of Eqs. (9)–(10). With the notation $\bar{j} = 1$ if $j = 2$ and $\bar{j} = 2$ if $j = 1$, this leads to

$$\rho_{j\infty} = A_j\delta_j\gamma, \quad a_{jj}\beta_j A_j + \ell_{12}a_{12}A_{\bar{j}}\gamma/2 = \ell_{12}a_{12}\rho_{\bar{j}\infty}\gamma, \quad j = 1,2 \tag{37}$$

where $\beta_j = (1/\ell_{jj} - 1/\ell_{12})^{-1} + (1/\ell_{jj} + 1/\ell_{12})^{-1}$, $\delta_j = (1/\ell_{jj} - 1/\ell_{12})^{-1}/\ell_{11}$, and $\gamma = \exp(-x_1/\ell_{12})$. Eliminating $A_{1,2}$ leads to a homogeneous system

$$\begin{pmatrix} a_{11}\beta_1/\delta_1 & \ell_{12}a_{12}(1/(2\delta_2 - 1)\gamma^2) \\ \ell_{12}a_{12}(1/(2\delta_1 - 1)\gamma^2) & a_{22}\beta_2/\delta_2 \end{pmatrix}\begin{pmatrix}\rho_{1\infty}\\ \rho_{2\infty}\end{pmatrix} = \begin{pmatrix}0\\0\end{pmatrix}. \tag{38}$$

Setting the determinant in (38) to zero gives

$$\gamma = 2\left(\frac{a_{11}a_{22}\ell_{11}\ell_{22}\ell_{12}^2}{a_{12}^2(\ell_{11}+\ell_{12})^2(\ell_{22}+\ell_{12})^2}\right)^{1/4}. \tag{39}$$

By the definition of γ, the assumption that $x_1 > 0$ requires $\gamma < 1$, which is fulfilled provided the inter-species interaction strength a_{12} is sufficiently large. Finally, the nullspace in (38) is characterized by pairs $(\rho_{1\infty}, \rho_{2\infty})$ satisfying

$$\frac{\rho_{1\infty}}{\rho_{2\infty}} = \left(\frac{a_{22}\ell_{22}}{a_{11}\ell_{11}}\right)^{1/2}, \tag{40}$$

which is the same as the energy balance requirement (15).

In general, no closed form expression for the critical potential K^* can be obtained, so checking the hypothesis of Proposition 2 would require numerical evaluation. On the other hand, in the restricted case for the Morse potential with $\ell_{11} = \ell_{22} = \ell_{12} = \ell$, $K^* = \sqrt{a_{11}a_{22}}\exp(-|x|/\ell)$, and the hypothesis $K^* < K_{12}$ is then equivalent to $\sqrt{a_{11}a_{22}} < a_{12}$.

2.6. Interface energy

The excess energy σ due to the presence of an interface can be defined by

$$\sigma = \min E_I(\rho_1, \rho_2) \tag{41}$$

where the minimization is over admissible states defined in Section 2.2. Notice that as long as E_I is bounded from below, this quantity is finite, independent of the existence of an actual interface profile. On the other hand, if there is a solution (ρ_1^*, ρ_2^*) to (9)–(10), these may be used to simplify the interface energy (16) to give the representations

$$\begin{aligned} \sigma &= \int e_0 - \frac{1}{2}\overline{\mu}_1\rho_1^* - \frac{1}{2}\overline{\mu}_2\rho_2^*\,dx \\ &= \int e_0 - \frac{1}{2}\rho_1^* K_{11} * \rho_1^* - \rho_1^* K_{12} * \rho_2^* - \frac{1}{2}\rho_2^* K_{22} * \rho_2^*\,dx. \end{aligned} \tag{42}$$

3. Domain interface evolution

In situations where segregation and domain formation is preferred, it is natural to describe the subsequent evolution of domain boundaries. The limiting case where domain sizes are much larger than the interaction length can be studied by scaling the interaction kernels as

$$K_{ij} = \epsilon^{-3}\overline{K}_{ij}(x/\epsilon), \quad \epsilon \ll 1$$

The scale of the prefactor depends both on the desired dynamic timescale as well as the spatial dimension. The specific choice here is made for dimension two, and so that the interface motion occurs on an $O(1)$ timescale. Extensions of the analysis to greater dimensions are straightforward.

A matched asymptotic expansion analogous to the Cahn–Hilliard equation [31] forms a basis for our investigation. It is useful to write (1)–(2) as

$$\frac{\partial\rho_i}{\partial t} = \nabla\cdot(\rho_i\nabla\mu_i), \quad \mu_i \equiv \epsilon^{-3}\left(\overline{K}_{ii} * \rho_i + \overline{K}_{i\bar{i}} * \rho_{\bar{i}}\right), \tag{43}$$

and seek expansions $\rho_i = \rho_{i,0} + \epsilon\rho_{i,1} + \epsilon^2\rho_{i,2} + \cdots$ and $\mu_i = \epsilon^{-1}\mu_{i,-1} + \mu_{i,0} + \epsilon\mu_{i,1} + \epsilon^2\mu_{i2} + \cdots$. The same notation will be used for the different expansions in the bulk (domain) and interface regions, unless ambiguity arises. Subdomains for which the leading order term $\rho_{i,0}$ are positive will be denoted Ω_i. Domain interfaces are notated $\Gamma = \partial\Omega_1/\partial\Omega = \partial\Omega_2/\partial\Omega$. The goal is to derive a problem describing the evolution of Γ.

3.1. Domain region expansion

In the region between interfaces it is imagined that ρ_i, μ_i vary on a $O(1)$ scale in space and time. This justifies the use of a moment expansion

$$K_{ij} * \rho_i = \epsilon^{-3}\int_{\mathbb{R}^2}\overline{K}_{ij}((x-y)/\epsilon)\rho_i(y)dy = \epsilon^{-1}M^0_{ij}\rho_0 + \epsilon M^2_{ij}\Delta\rho_i(x) + \cdots \tag{44}$$

where

$$M^n = \frac{1}{n!}\int_{\mathbb{R}^2} \overline{K}(z)|z|^n dz.$$

Observe here that the odd expansion terms vanish due to radial symmetry.

The leading order problem is

$$0 = \nabla\cdot(\rho_{i,0}\nabla\mu_{i,-1}), \quad \mu_{i,-1} = M^0_{ii}\rho_{i,0} + M^0_{i\bar{i}}\rho_{\bar{i},0}, \quad i = 1,2, \tag{45}$$

satisfied on subdomains Ω_i, together with the boundary condition $\nabla\mu_{i,-1}\cdot\boldsymbol{n} = 0$. In addition, matching to the interface region provides the conditions

$$\rho_{i,0} = \begin{cases} \rho_{i\infty}, & \text{on } \partial\Omega_i, \\ 0 & \text{on } \partial\Omega_{\bar{i}}. \end{cases} \tag{46}$$

The solution to the system (45) in each subdomain is therefore

$$\rho_{i,0} = \begin{cases} \rho_{i\infty}, & \text{in } \Omega_i, \\ 0, & \text{otherwise.} \end{cases} \tag{47}$$

where

$$\mu_{i,-1} = \begin{cases} M^0_{ii}\rho_{i\infty}, & \text{in } \Omega_i, \\ M^0_{i\bar{i}}\rho_{\bar{i}\infty}, & \text{otherwise.} \end{cases} \tag{48}$$

For arbitrary initial conditions of (1)–(2), relaxation toward this leading order solution occurs on a faster timescale which is not considered here.

The next order in the expansion describes the correction term in μ, specifically $\Delta\mu_{i,0} = 0$ to be solved on each component of Ω_i. This is supplemented with conditions $\nabla\mu_{i,0}\cdot\boldsymbol{n} = 0$ on $\partial\Omega$ and a Dirichlet condition on Γ given by matching to the interface region. The solution of this steady state diffusion equation provides boundary data for the interface velocity equation (80).

3.2. Interface region expansion

To capture the geometry of the curved interface, a standard fitted/scaled coordinate system is used. Letting $\gamma(s)$ be the (assumed smooth) parameterization of the interface, then at least locally it is possible to write $\boldsymbol{x} = \gamma(s) + r\boldsymbol{n}(s)$ where $\boldsymbol{n}$ is the normal to the interface. The Jacobian determinant of the coordinate transformation $\boldsymbol{x} \to (r,s)$ is $1 - r\kappa(s)$ where the interface curvature κ is positive when $\boldsymbol{n}$ is in the direction of the convex region bounded by the interface. The convention is used here that $\boldsymbol{n}$ points toward the Ω_1 subdomain. The interface region will employ the coordinates $(z,s) = (r/\epsilon, s)$, anticipating that the solution profile varies rapidly only in the direction normal to the interface. For notational convenience, we also define $q = s/\epsilon$.

By choice of expansions, the leading order ($O(\epsilon^{-3})$) term for ((43)a) in local scaled coordinates reads

$$\frac{\partial}{\partial z}\left(\rho_{i,0}\frac{\partial\mu_{i,-1}}{\partial z}\right) = 0, \tag{49}$$

with

$$\begin{aligned} &\mu_{i,-1} = \tilde{K}_{ii}(z) * \rho_{i,0}(z) + \tilde{K}_{i\bar{i}}(z) * \rho_{\bar{i},0}(z), \\ &\tilde{K}(z) \equiv \int \overline{K}(q\boldsymbol{t}(0) + z\boldsymbol{n}(0))dq, \quad \boldsymbol{t}(s) = \gamma'(s). \end{aligned} \tag{50}$$

The notation $\tilde{K}$ refers to the reduced potential

$$\tilde{K}(z) \equiv \int \overline{K}(q\boldsymbol{t}(0) + z\boldsymbol{n}(0))dq, \quad \boldsymbol{t}(s) = \gamma'(s),$$

i.e. the interaction kernel integrated over the direction transverse to the interface. The system (49)–(50) is equivalent to the interface problem discussed in Section 2. Specifically, $\mu_{i,-1}$ must be constant on the support of $\rho_{i,0}$, and the choice of direction of $\boldsymbol{n}$ gives the correct asymptotic values for ρ_i as $z \to \pm\infty$.

The $O(\epsilon^{-2})$ expansion term for ((43)a) is

$$\frac{\partial}{\partial z}\left(\rho_{i,0}\frac{\partial\mu_{i,0}}{\partial z}\right) = 0, \tag{51}$$

which means that $\mu_{i,0}$ is a constant on the support of $\rho_{i,0}$ (this uses that fact that $\partial\mu_{i,0}/\partial z$ matches the normal derivative of $\mu_{i,-1}$ in the domain region). The correction terms for the nonlocal equations provide a linear system

$$\begin{aligned} &\tilde{K}_{ii}(z) * \rho_{i,1}(z) + \tilde{K}_{i\bar{i}}(z) * \rho_{\bar{i},1}(z) = \\ &\mu_{i,0} - \kappa \iint \left(\frac{1}{2}\frac{\partial\overline{K}_{ii}}{\partial z}q^2 - z\overline{K}_{ii}\right)\rho_{i,0} \\ &\quad + \left(\frac{1}{2}\frac{\partial\overline{K}_{i\bar{i}}}{\partial z}q^2 - z\overline{K}_{i\bar{i}}\right)\rho_{\bar{i},0}\, dz dq, \quad i = 1,2, \end{aligned} \tag{52}$$

where $\overline{K}(z,q)$ is shorthand for $\overline{K}(q\boldsymbol{t}(0) + z\boldsymbol{n}(0))$ and $\kappa = \kappa(0)$. This represents a self-adjoint system of equations for $\rho_{1,1}$ and $\rho_{1,2}$. Supposing that the leading order solutions are differentiable almost everywhere, it is easy to check that $(\rho'_{1,0}, \rho'_{2,0})$ is in the kernel of this operator. Solvability is therefore provided by taking inner products, resulting in

$$\mu_{1,0}\rho_{1\infty} - \mu_{2,0}\rho_{2\infty} = \kappa\sigma, \tag{53}$$

where

$$\begin{aligned} \sigma = &\iiint \left(\frac{1}{2}\frac{\partial\overline{K}_{11}}{\partial z}(z-z_0,q)q^2 - z\overline{K}_{11}(z-z_0,q)\right)\rho_{1,0}(z)\rho'_{1,0}(z_0) \\ &+ 2\left(\frac{1}{2}\frac{\partial\overline{K}_{12}}{\partial z}(z-z_0,q)q^2 - z\overline{K}_{12}(z-z_0,q)\right)\rho_{1,0}(z)\rho'_{2,0}(z_0) \\ &+ \left(\frac{1}{2}\frac{\partial\overline{K}_{22}}{\partial z}(z-z_0,q)q^2 - z\overline{K}_{22}(z-z_0,q)\right)\rho_{2,0}(z)\rho'_{2,0}(z_0)\, dq\, dz\, dz_0. \end{aligned} \tag{54}$$

The constant σ may be interpreted as interfacial energy as follows. Integration by parts in z_0 produces

$$\begin{aligned} \sigma = &\iiint \left(\frac{1}{2}\frac{\partial^2\overline{K}_{11}}{\partial z^2}(z-z_0,q)q^2 - z\frac{\partial\overline{K}_{11}}{\partial z}(z-z_0,q)\right)\rho_{1,0}(z)(\rho_{1,0}(z_0) - \rho_{1\infty}) \\ &+ 2\left(\frac{1}{2}\frac{\partial^2\overline{K}_{12}}{\partial z^2}(z-z_0,q)q^2 - z\frac{\partial\overline{K}_{12}}{\partial z}(z-z_0,q)\right)\rho_{1,0}(z)\rho_{2,0}(z_0) \\ &+ \left(\frac{1}{2}\frac{\partial^2\overline{K}_{22}}{\partial z^2}(z-z_0,q)q^2 - z\frac{\partial\overline{K}_{22}}{\partial z}(z-z_0,q)\right) \\ &\times \rho_{2,0}(z)(\rho_{2,0}(z_0) - \rho_{2\infty})\, dq\, dz\, dz_0. \end{aligned} \tag{55}$$

After integration in q, the terms involving $zK()$ may be written

$$\int z\rho_{1,0}(z)(\tilde{K}_{11} * \rho_{1,0} + \tilde{K}_{12} * \rho_{2,0})_z + z\rho_{2,0}(z)(\tilde{K}_{22} * \rho_{2,0} + \tilde{K}_{12} * \rho_{1,0})_z\, dz, \tag{56}$$

which vanishes by virtue of (50). In order to simplify the remainder, we use radial symmetry and let $\overline{K}(z,q) = f(z^2+q^2)$. Differentiation once and twice gives

$$\begin{aligned} &\overline{K}_z = 2zf', \quad \overline{K}_q = 2qf', \quad q^2\overline{K}_{zz} = 4z^2q^2f'' + 2f'q^2, \\ &z^2\overline{K}_{qq} = 4z^2q^2f'' + 2f'q^2, \end{aligned} \tag{57}$$

therefore

$$q^2\overline{K}_{zz} = q\overline{K}_q - z\overline{K}_z + z^2\overline{K}_{qq}. \tag{58}$$

Using this in (55) and integrating over q produces

$$\begin{aligned}\sigma = &-\iint \frac{1}{2}\tilde{K}_{11}(z-z_0)\rho_{1,0}(z)(\rho_{1,0}(z_0)-\rho_{1\infty})+\tilde{K}_{12}(z-z_0)\rho_{1,0}(z)\rho_{2,0}(z_0)\\ &+\frac{1}{2}\tilde{K}_{22}(z-z_0)\rho_{2,0}(z)(\rho_{2,0}(z_0)-\rho_{2\infty})\,dz\,dz_0\\ &-\iint (z-z_0)\Big(\frac{1}{2}\tilde{K}'_{11}(z-z_0)\rho_{1,0}(z)\rho_{1,0}(z_0)+\tilde{K}'_{12}(z-z_0)\rho_{1,0}(z)\rho_{2,0}(z_0)\\ &+\frac{1}{2}\tilde{K}'_{22}(z-z_0)\rho_{2,0}(z)\rho_{2,0}(z_0)\Big)\,dz\,dz_0\\ &+\frac{1}{2}\iint (z-z_0)\Big(\tilde{K}'_{11}(z-z_0)\rho_{1,0}(z)\rho_{1\infty}+\tilde{K}'_{22}(z-z_0)\rho_{2,0}(z)\rho_{2\infty}\Big)dz\,dz_0.\end{aligned} \tag{59}$$

The second integral can be written similar to (56), and therefore vanishes. The last term can be evaluated (recalling the definitions of $\mu_{1,2}$) as $-\frac{1}{2}\int \mu_1\rho_{1,0}+\mu_2\rho_{2,0}\,dz$, so that finally

$$\sigma = \int e_0 - \frac{1}{2}\rho_{1,0}\tilde{K}_{11} * \rho_{1,0} - \rho_{1,0}\tilde{K}_{12} * \rho_{2,0} - \frac{1}{2}\rho_{2,0}\tilde{K}_{22} * \rho_{2,0}\ dz. \tag{60}$$

Notice this agrees with the domain interface surface energy given in (42).

Further expansion of ((43)a) gives

$$-V_n\frac{\partial\rho_{i,0}}{\partial z} = \frac{\partial}{\partial z}\left(\rho_{i,0}\frac{\partial\mu_{i,1}}{\partial z}\right), \tag{61}$$

where the negative normal interface velocity $-V_n$ has been identified with the time derivative of the moving coordinate r. Integration gives $V_n = -\partial\mu_{1,1}/\partial z = -\partial\mu_{2,1}/\partial z$, and matching to the outer solution gives two expressions for V_n,

$$V_n = -\nabla\mu_{1,0}\cdot\boldsymbol{n} = -\nabla\mu_{2,0}\cdot\boldsymbol{n}, \tag{62}$$

where the normal derivatives of μ_i are one-sided limits, taken from the direction of the subdomain Ω_i.

3.3. Boundary layers and the Laplace-Young condition

Repulsive interactions can produce concentration of density near the system boundary. This gives rise to an excess energy associated with the boundary, and leads to an expression for the contact angle at the junction of domain interfaces and system boundaries.

To investigate the density boundary layer, consider a rectilinear local coordinates (r,s), defined so that the origin is on the (assumed smooth) system domain boundary and r is normal to the boundary. Different expansions are sought depending on whether the origin is in the closure of one subdomain Ω_i, or at a triple junction where Γ meets the boundary.

For the first case, the scaled coordinate $z = r/\epsilon$ is employed, and the leading order boundary layer solutions, labeled ρ_i^b, satisfy

$$\int_0^\infty \tilde{K}_{ii}(z-\zeta) * \rho_i^b(\zeta)d\zeta = \mu_{i,-1}, \quad z\geq 0, \quad \rho_{i,0}(\infty) = \rho_{i\infty}, \tag{63}$$

where $\mu_{i,-1}$ and $\tilde{K}$ are defined as before. This represents a standard Fredholm integral equation of the first kind. Solutions to such equations do not need to be smooth or classical; indeed it is known that point concentrations may be present on domain boundaries in one species aggregation equations [7]. For example, for the potential $\tilde{K}(z) = \exp(-|z|)$, it can be checked that $\rho_i = \rho_{i\infty}(1+\delta(x))$ is the solution.

An alternative characterization of Eq. (63) is obtained by minimization of

$$\begin{aligned}E_i^b(\rho) = &\int_0^\infty\int_0^\infty \frac{1}{2}\tilde{K}_{ii}(z-\zeta)\rho(z)\rho(\zeta)\,dz\,d\zeta\\ &-\int_0^\infty \mu_{i,-1}\rho(z)+e_0\,dz, \quad e_0 = M_{ii}^0\rho_{i\infty}^2/2,\end{aligned} \tag{64}$$

over nonnegative measures ρ with the far field condition in (63). We will suppose this problem admits a unique solution $\rho_{i,0}$. The excess energy (per unit length) of the boundary layer can then be defined as $\sigma_i \equiv E_i^b(\rho_i^b)$.

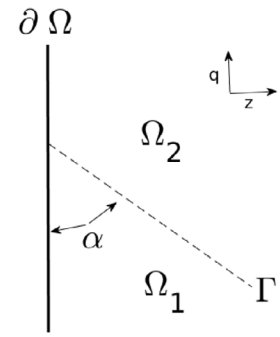

Fig. 2. Configuration for junction of domain interface and domain boundary.

The region where the domain interface Γ intersects the boundary requires the use of the (fully) scaled coordinates $(z,q) = \epsilon^{-1}(r,s)$. We suppose that Γ intersects the boundary with contact angle α, and the subdomains $\Omega_{1,2}$ are configured as in Fig. 2. It is useful to extend the domain to $(z,q)\in\mathbb{R}^2$ by setting ρ_1,ρ_2 equal to zero for $z<0$, so that the leading order problem is

$$\overline{K}_{11} * \rho_{1,0} + \overline{K}_{12} * \rho_{2,0} = \mu_{1,-1}, \quad (z,q)\in \mathrm{spt}\rho_{1,0}, \tag{65}$$

$$\overline{K}_{12} * \rho_{1,0} + \overline{K}_{22} * \rho_{2,0} = \mu_{2,-1}, \quad (z,q)\in \mathrm{spt}\rho_{2,0}. \tag{66}$$

Matching to the boundary and interface layers requires

$$\rho_i(q,z) \sim \rho_1^b(z), \quad q\to\infty, \quad z = O(1), \tag{67}$$

$$\rho_i(q,z) \sim \rho_2^b(z), \quad q\to-\infty, \quad z = O(1), \tag{68}$$

$$\rho_i(q,z) \sim \rho_i^{int}(x), \quad z\to\pm\infty, \quad -z/q\sim\tan\alpha. \tag{69}$$

where $x = z\cos\alpha + q\sin\alpha$ is the rotated coordinate transverse to the domain interface and ρ^{int} is the interface profile.

A solvability condition for this system is given by ensuring the variation of energy with respect to translation of the contact point along $\partial\Omega$ vanishes. This is accomplished by multiplying (65)–(66) by $\partial\rho_1/\partial q$ and $\partial\rho_2/\partial q$, respectively, summing and integrating. Although (65)–(66) are only valid on the respective supports, the domain of integration may be extended to a large semicircle C_L of radius L, giving

$$\begin{aligned}\int_0^L\int_{-\sqrt{L^2-z^2}}^{\sqrt{L^2-z^2}} &\rho_{1q}\overline{K}_{11} * \rho_1 + \rho_{2q}\overline{K}_{12} * \rho_1 + \rho_{1q}\overline{K}_{12} * \rho_2 + \rho_{2q}\overline{K}_{22} * \rho_2\\ &- \mu_{1,-1}\rho_1 - \mu_{2,-1}\rho_2\,dq\,dz = 0.\end{aligned} \tag{70}$$

Integration by parts (in q and then in the convolution) can be used to verify the formulas

$$\begin{aligned}&\int_{C_L}\rho_q K * \rho\ dz\,dq \sim \frac{1}{2}\int_{C_L}(\rho K * \rho)_q\ dz\,dq,\\ &\int_{C_L}\rho_{1q}K * \rho_2 + \rho_{2q}K * \rho_1\ dz\,dq \sim \int_{C_L}(\rho_1 K * \rho_2)_q\ dz\,dq,\end{aligned} \tag{71}$$

for $L\to\infty$. Using these in (70) produces

$$\begin{aligned}\int_0^L \Big[&\frac{1}{2}\rho_1\overline{K}_{11} * \rho_1 + \rho_2\overline{K}_{12} * \rho_1 + \frac{1}{2}\rho_2\overline{K}_{22} * \rho_2\\ &- \mu_{1,-1}\rho_1 - \mu_{2,-1}\rho_2 + e_0\Big]_{q=-\sqrt{L^2-z^2}}^{q=\sqrt{L^2-z^2}}\,dz \sim 0,\end{aligned} \tag{72}$$

for $L\to\infty$. Using matching condition (67), the $q = \sqrt{L^2-z^2}$ term is the same as (64) as $L\to\infty$, in other words it gives the boundary layer energy σ_1. The $q = -\sqrt{L^2-z^2}$ term must be matched both for $z = O(1)$ and $z = O(L)$ with $\sqrt{L^2-z^2} = -q\sim z/(\tan\alpha)$. The former produces σ_2

and the latter gives

$$\int_0^L \frac{1}{2}\rho_1^{int}\overline{K}_{11} * \rho_1^{int} + \rho_2^{int}\overline{K}_{12} * \rho_1^{int} + \frac{1}{2}\rho_2^{int}\overline{K}_{22} * \rho_2^{int} - \mu_{1,-1}\rho_1^{int} - \mu_{2,-1}\rho_2^{int} + e_0\, dz, \tag{73}$$

where the interface profiles are evaluated at $x = z\cos\alpha - \sqrt{L^2 - z^2}\sin\alpha$. Changing the variable of integration to x and noting that as $L \to \infty$, $dx = \cos\alpha - z/\sqrt{L^2 - z^2}\sin\alpha\, dz \sim \cos\alpha + \tan\alpha\sin\alpha\, dz = \sec\alpha\, dz$, the limiting value of (73) is

$$\cos\alpha \int_{-\infty}^{\infty} \frac{1}{2}\rho_1^{int}\overline{K}_{11} * \rho_1^{int} + \rho_2^{int}\overline{K}_{12} * \rho_1^{int} + \frac{1}{2}\rho_2^{int}\overline{K}_{22} * \rho_2^{int} - \mu_{1,-1}\rho_1^{int} - \mu_{2,-1}\rho_2^{int} + e_0\, dx. \tag{74}$$

which is the interface energy (16). In other words, as $L \to \infty$ expression (72) becomes

$$\sigma_2 - \sigma_1 - \sigma\cos\alpha = 0, \tag{75}$$

which is the well-known Laplace–Young condition.

3.4. Free boundary problem

The forgoing computation can be summarized as a free boundary problem for the motion of domain interfaces. Letting μ_i denote the outer expansion terms $\mu_{i,0}$, the complete problem is

$$\Delta\mu_1 = 0, \quad \text{on } \Omega_1, \tag{76}$$

$$\Delta\mu_2 = 0, \quad \text{on } \Omega_2, \tag{77}$$

$$\rho_{1\infty}\mu_1 - \rho_{2\infty}\mu_2 = \sigma\kappa, \quad \text{on } \Gamma, \tag{78}$$

$$\nabla\mu_1 \cdot \boldsymbol{n} = 0, \quad \nabla\mu_2 \cdot \boldsymbol{n} = 0, \quad \text{on } \partial\Omega. \tag{79}$$

$$V_n = -\nabla\mu_1 \cdot \boldsymbol{n} = -\nabla\mu_2 \cdot \boldsymbol{n}. \tag{80}$$

together with (75) where Γ and $\partial\Omega$ intersect.

Define the total interfacial/boundary energy as

$$E_0 = \int_\Gamma \sigma\, ds + \int_{\partial\Omega\cup\partial\Omega_1} \sigma_1\, ds + \int_{\partial\Omega\cup\partial\Omega_2} \sigma_2\, ds. \tag{81}$$

The rate of energy dissipation is

$$\frac{dE_0}{dt} = -\int_\Gamma \sigma\kappa V_n\, dx \tag{82}$$

$$= \int_\Gamma \rho_{1\infty}\mu_1\nabla\mu_1 \cdot \boldsymbol{n} - \rho_{2\infty}\mu_2\nabla\mu_2 \cdot \boldsymbol{n}\, dx \tag{83}$$

$$= -\rho_{1\infty}\int_{\Omega_1} |\nabla\mu_1|^2 dx - \rho_{2\infty}\int_{\Omega_2} |\nabla\mu_2|^2 dx. \tag{84}$$

The first equality depends on (75), so that no energy is dissipated as the contact point moves along the boundary. This computation suggests that E_0 is the correct candidate for the Γ-limit energy, and that the $\epsilon \to 0$ limit and the gradient flow dynamics commute.

Notice that, in contrast to the classical Mullins–Sekerka free boundary problem for phase segregation [32], problem (76)–(80) has two expressions for the interface velocity. This is compensated by the fact that there is a single boundary condition for both fields μ_1, μ_2. The well-posedness of the boundary value problem is demonstrated in the next result.

Proposition 3. *Suppose that Γ is C^1. There exists a solution to (76)–(78) for which the second equality in (80) is satisfied.*

Proof. Consider the functional

$$D(\mu_1, \mu_2) = \rho_{1\infty}\int_{\Omega_1} |\nabla\mu_1|^2 dx + \rho_{2\infty}\int_{\Omega_2} |\nabla\mu_2|^2 dx,$$

for $\mu_i \in H^1(\Omega_i)$, which also satisfy the interface condition (78) in the trace sense. The direct method of the calculus of variations establishes the existence of a minimizer (μ_1^*, μ_2^*) satisfying (76)–(77), and moreover $\mu_{1,2}^* \in C_1$ by classical regularity results. The first variation is computed as

$$\delta D = -\rho_{1\infty}\int_{\Omega_1} \delta\mu_1\Delta\mu_1^* dx - \rho_{2\infty}\int_{\Omega_2} \delta\mu_2\Delta\mu_2^* dx + \int_\Gamma \rho_{1\infty}\delta\mu_1\nabla\mu_1^* \cdot \boldsymbol{n} - \rho_{2\infty}\delta\mu_2\nabla\mu_2^* \cdot \boldsymbol{n}\, dx \tag{85}$$

for all admissible perturbations $\delta\mu_{1,2}$. By (78) these must satisfy

$$\delta\mu_1\rho_{1\infty} - \delta\mu_2\rho_{2\infty} = 0, \quad x \in \Gamma. \tag{86}$$

Since the first variation must vanish, it follows that $\nabla\mu_1 \cdot \boldsymbol{n} - \nabla\mu_2 \cdot \boldsymbol{n} = 0$ on Γ. □

4. Domain coarsening and dynamic scaling

Since the dynamics described by (76)–(80) is driven by surface energy alone, it is reasonable to expect that domains will grow over time. The mechanisms for this process are somewhat different than classical Ostwald ripening [33], however, since there is no diffusion of material through the domain of the opposite species.

It is instructive to consider a domain configuration where the first species occupies several circular domains with radii $R_1, R_2, \ldots$. For diffusion driven coarsening, larger domains will grow at the expense of smaller ones. Here, however, such a configuration is a steady state. Indeed, the solution of (76)–(78) is (up to additive constants)

$$\mu_1 = 0, \quad \mu_2 = -\frac{\sigma}{R_i\rho_{2\infty}} \text{ on circle } i. \tag{87}$$

and therefore the interface velocities are zero.

In general, we find that domain growth in the present model is still possible, but is related to global rearrangements of interfaces. This is investigated next, using numerical computations of both the particle and continuum systems.

4.1. Particle system dynamics

The system (4) was simulated using straightforward explicit timestepping. The potentials were $K_{11}(x) = K_{22}(|x|) = e^{-|x|/a}$ and $K_{12} = e^{-|x|/b}$ with $a = 3$ and $b = 4$. A domain of size 200^2 was used, and periodic boundary conditions were employed. The distance between two particles was taken to be the minimum distance between periodic copies; since the interaction length scales a, b are much smaller than the system size, this does not have any meaningful effect on the potential.

For equal mass fraction $N_x = N_y = 2500$, the resulting segregation process is shown in Fig. 3. Notice the final configuration represents a single interface, wrapped twice around the torus. Unequal mass fraction ($N_x = 4000$, $N_y = 1000$) was also investigated (Fig. 3,bottom). In this case, the system tends toward the multiple circle configuration described above.

4.2. Continuum system

Eqs. (1)–(2) were also simulated, using the same potentials and domain. The convolution terms were computed by Fourier transform, assuming a uniform grid and periodic boundary conditions. Timestepping used upwind differences, with a step limiter to prevent negative solutions. Initial conditions were set equal to one plus a small random perturbation.

Fig. 4 shows the results for equal and unequal (20%–80%) mass fractions. The results were qualitatively similar to the particle dynamics, and the timescales for coarsening were similar as well.

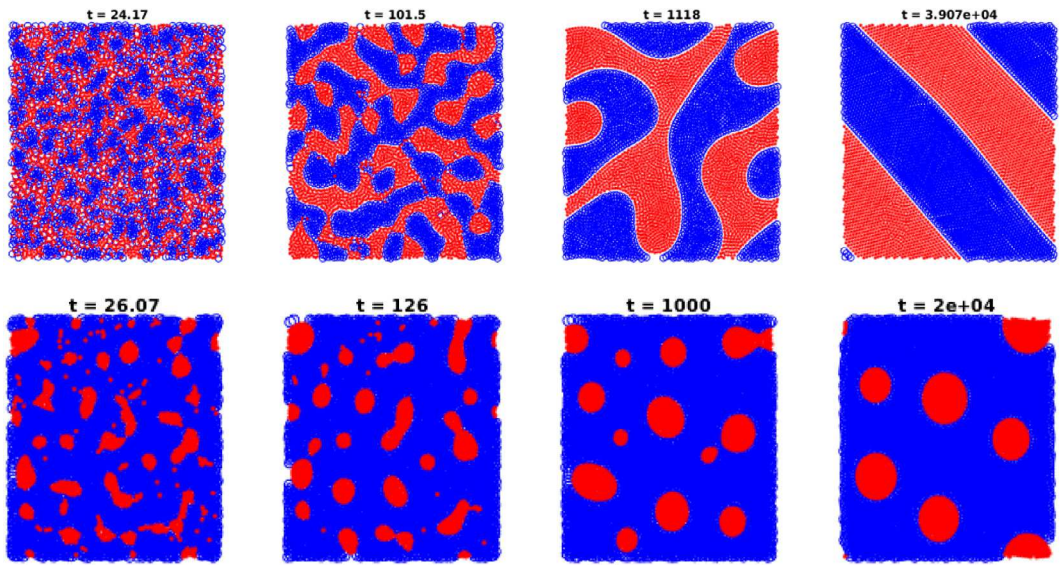

Fig. 3. Simulations of particle system (4). Top: $N_x = N_y = 2500$. Bottom: $N_x = 4000$, $N_y = 1000$.

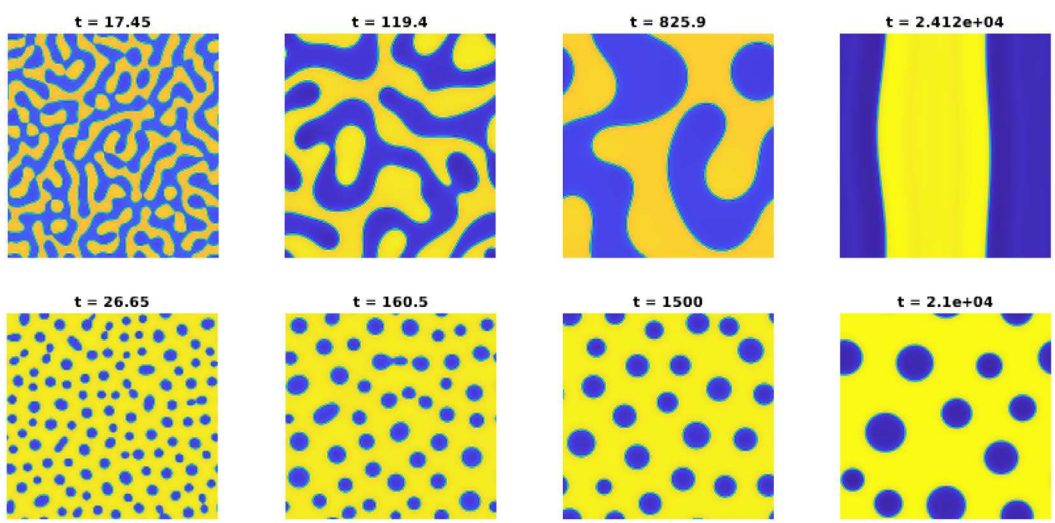

Fig. 4. Simulations of continuum Eqs. (1)–(2). Shown is a color map of the difference $\rho_1 - \rho_2$. Top: Equal mass ratio. Bottom: Mass ratio 4:1.

4.3. Evolution of lengthscales

The coarsening process can be quantified by observing how pattern lengthscales change over time. For the particle system, we define the dynamic pattern lengthscale via the metric

$$\ell_p \equiv \frac{1}{2N_x}\sum_{i=1}^{N_x}\min_j |X_i - Y_j| + \frac{1}{2N_y}\sum_{i=1}^{N_y}\min_j |X_j - Y_i|. \tag{88}$$

For the continuum system, it is convenient to use the power spectrum of one component (ρ_1 here) given by $|\hat{\rho}_1(k)|^2$, which for systems possessing a definite wavelength is mostly concentrated at wavenumbers of a certain magnitude. We can therefore define a lengthscale by taking a reciprocal of the spectral average of wavenumbers, given by

$$l_p \equiv \frac{\int |\hat{\rho}_1(k)|^2 dk}{\int |\hat{\rho}_1(k)|^2 |k| dk}. \tag{89}$$

Simulation data was used to compute the lengthscales as a function of time (Fig. 5). For the particle system, there is transient behavior when the interaction and domain lengthscales are similar in size, which gives way to a power-law type scaling. In contrast to Ostwald ripening behavior which is typically characterized by the dynamic scaling law $\ell \sim t^{1/3}$, this does not seem to be the case here. An empirical fit of $\ell \sim t^{1/4}$ seems to be better, as shown in Fig. 5.

Note that the transient behavior is not captured by the analysis of Section 3, and so the crossover of dynamics is not surprising. In addition, as the pattern length becomes comparable to the system size, there is also a slowing of the dynamics.

The effect of different mass ratios is also shown in Fig. 5. Whereas early time behavior is similar, the dilute system shows dramatic slowing as the separation distance between connected subdomains becomes larger than the interaction length.

5. Long range effects

The interplay between short- and long-ranged interactions has been studied for some time, both in the context of physical models [34–37]

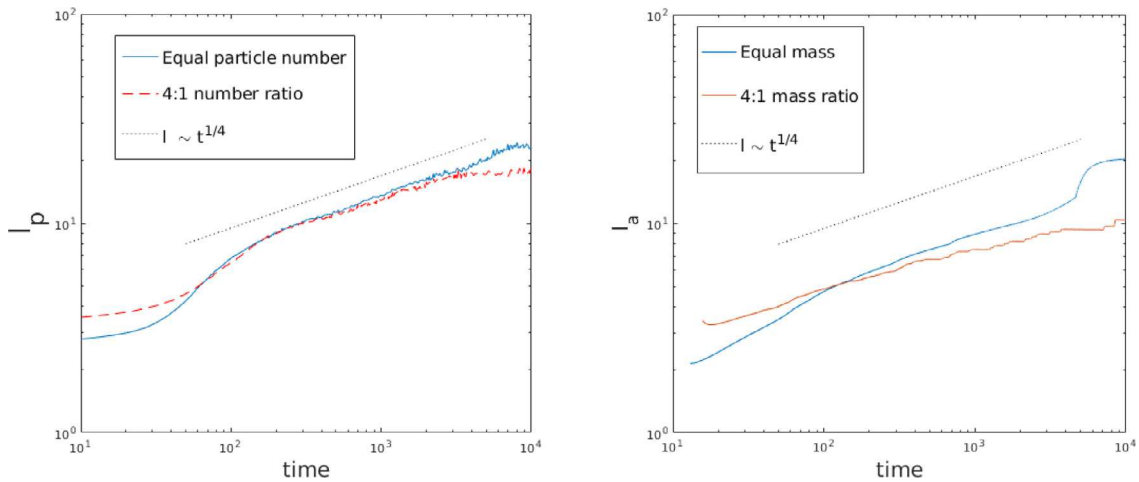

Fig. 5. Left: dynamics of particle model lengthscale (88) for the two cases in Fig. 3. Right: dynamics of lengthscale for continuum model (89). In both cases, a line representing $t^{1/4}$ power-law behavior is shown for comparison.

and aggregation equations [7,22,38,39]. These often result in complex pattern formation such as cluster phases, labyrinthine structures, and density concentration on sets of lower dimension.

In this section the energy is modified by the addition of long-range components

$$E_2 = \int_\Omega \frac{1}{2}\rho_1(K_{11}+L_{11}) * \rho_1 + \frac{1}{2}\rho_2(K_{22}+L_{22}) * \rho_2 + \rho_1(K_{12}+L_{12}) * \rho_2 \, dx. \tag{90}$$

The potentials L_{ij} vary on an $O(1)$ lengthscale, and are assumed integrable. They need not be positive, however; choosing $L_{ij} < 0$ implies attraction between species i and j.

5.1. Modified free boundary problem

In the context of the asymptotic analysis of Section 3, the term involving L would appear in the correction term Eq. (52). This produces a modification to the interface condition (78) in the free boundary problem (76)–(80)

$$\begin{aligned}\sigma\kappa &= \rho_{1\infty}(\mu_1 - L_{12} * \rho_{2,0} - L_{11} * \rho_{1,0}) - \rho_{2\infty}(\mu_2 - L_{12} * \rho_{1,0} - L_{22} * \rho_{2,0}) \\ &\equiv \rho_{1\infty}\mu_1 - \rho_{2\infty}\mu_2 + \rho_{2\infty}(\rho_{2\infty}L_{22} - \rho_{1\infty}L_{12}) * \chi_2 \\ &\quad - \rho_{1\infty}(\rho_{1\infty}L_{11} - \rho_{2\infty}L_{12}) * \chi_1, \quad \text{on } \Gamma,\end{aligned} \tag{91}$$

where $\chi_i = \chi(\Omega_i)$ and $\rho_{i,0}$ refers to the outer solution. Notice that the potentials can be redefined to absorb L_{12}, by replacing L_{11} with $L_{11} - \rho_{2\infty}L_{12}/\rho_{1\infty}$ and L_{22} with $L_{22} - \rho_{1\infty}L_{12}/\rho_{2\infty}$. An important consequence of this observation is that long range *inter*species attraction behaves the same as *intra*species repulsion.

The limiting energy (81) is now

$$E_0 = \int_\Gamma \sigma \, dx + \sum_{i,j=1}^{2} \frac{\rho_{i\infty}\rho_{j\infty}}{2} \int_{\Omega_i}\int_{\Omega_j} L_{ij}(x-y)dxdy.$$

This is dissipated in the same way as before:

$$\begin{aligned}\frac{dE_0}{dt} &= \int_\Gamma \Big[-\sigma\kappa + \rho_{2\infty}(-\rho_{1\infty}L_{12} + \rho_{2\infty}L_{22}) * \chi_2 \\ &\quad - \rho_{1\infty}(-\rho_{2\infty}L_{12} + \rho_{1\infty}L_{11}) * \chi_1 \Big] V_n \, dx \qquad (92)\\ &= \int_\Gamma \rho_{1\infty}\mu_1 \nabla\mu_1 \cdot \boldsymbol{n} - \rho_{2\infty}\mu_2\nabla\mu_2 \cdot \boldsymbol{n} \, dx \qquad (93)\\ &= -\rho_{1\infty}\int_{\Omega_1} |\nabla\mu_1|^2 dx - \rho_{2\infty}\int_{\Omega_2} |\nabla\mu_2|^2 dx. \qquad (94)\end{aligned}$$

5.2. Numerical illustrations

The role of long-range interspecies attraction given by

$$L_{12}(x) = -A\exp(-|x|/\ell), \quad \ell = 30, \tag{95}$$

is illustrated by numerical simulations of the continuum system (1)–(2). By the observations of the previous section, this is asymptotically equivalent to long-ranged self- repulsion of each species. The short-ranged potentials used here are the same as in Section 4.

Random initial conditions with either equal or unequal (4:1) mass fraction were used, and the domain was 800 × 800. The initial development of interfaces and distinct domains is similar to those shown in Section 4, but the subsequent equilibration is profoundly different.

Fig. 6 shows steady state equilibria for cases where $A = 0.02$. When the mass of both species is equal, phase domains organize in a labyrinthine fashion, and subsequently do not exhibit significant coarsening effects. Where there is a significant preponderance of one species, on the other hand, isolated domains undergo very little coarsening.

When the magnitude of the long range attraction is larger, the asymptotic description is no longer valid. In particular, short range repulsion can be overcome by attraction, leading to condensation of phases into localized patterned aggregates surrounded by empty space. Fig. 7 illustrates this phenomenon in the case where $A = 0.05$. Several isolated regions emerge, and gradually coalesce as a result of attraction. At late stages, this process becomes exceedingly slow due to the exponential nature of the potential.

6. Conclusions

Repulsive interparticle interactions in confined systems can lead to domain formation, akin to classical descriptions of material phase segregation. Here, this is an effect stemming from dominant interspecies repulsion, rather than a two-well energy potential which penalizes mixing. Domain interfaces have associated excess energy, and therefore exhibit surface tension effects. Dynamically this manifests as material flux which stems from gradients of the "chemical potentials" μ_i that arise from spatially varying interface curvature. This ultimately drives coarsening effects and pattern formation.

The model described here diverges from traditional continuum models for phase separation [28] in significant ways. There, interparticle interactions are effectively approximated by a phenomenological gradient energy term (or a nonlocal variant [29]), which opposes segregation effects. The resulting dynamics are different as well: here there is no diffusion of material through the other phase's domain, inhibiting coarsening effects.

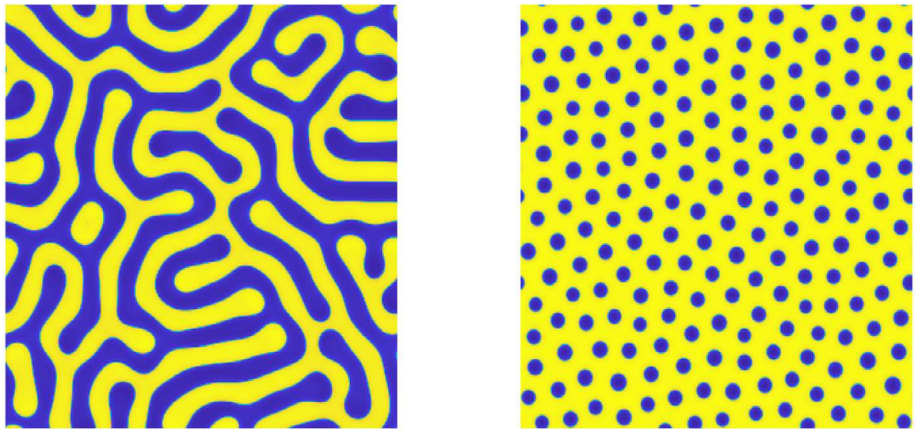

Fig. 6. Equilibrium behavior when a modest amount of long range interspecies attraction is included. The difference $\rho_1 - \rho 2$ is shown. Left: Equal mass, Right: mass ratio of 4:1.

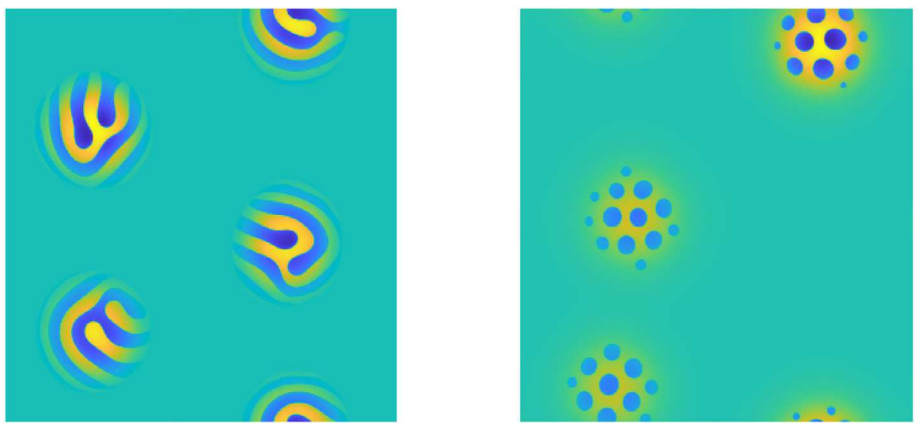

Fig. 7. Near -equilibrium behavior for large magnitude interspecies attraction. The free boundary description no longer applies, and patterned aggregates emerge. The difference $\rho_1 - \rho_2$ is shown. Left: Equal mass, Right: mass ratio of 4:1.

The present study points to a number of challenges and opportunities. A more complete analysis of the interface problem should be possible, although the absence of regularizing effects like diffusion makes this complicated (e.g. [40]). A natural sequel to such a study would be a precise understanding of the limiting energy in the sense of Γ-convergence [41,42]. Finally, the connection between the interparticle system, continuum limit, and free boundary problem provides significant avenues for pattern prediction and numerical simulation.

CRediT authorship contribution statement

Karl Glasner: Conceptualization, Formal analysis, Funding acquisition, Methodology, Project administration, Software, Visualization, Writing, Editing.

Declaration of competing interest

The authors declare that they have no known competing financial interests or personal relationships that could have appeared to influence the work reported in this paper.

Data availability

Data will be made available on request.

Acknowledgment

The author was supported through National Science Foundation award DMS-1908968.

References

[1] Silvia Boi, Vincenzo Capasso, Daniela Morale, Modeling the aggregative behavior of ants of the species polyergus rufescens, Nonlinear Anal. RWA 1 (1) (2000) 163–176.
[2] Alexander Mogilner, Leah Edelstein-Keshet, A non-local model for a swarm, J. Math. Biol. 38 (6) (1999) 534–570.
[3] Chad M. Topaz, Andrea L. Bertozzi, Mark A. Lewis, A nonlocal continuum model for biological aggregation, Bull. Math. Biol. 68 (7) (2006) 1601.
[4] Thomas Laurent, Local and global existence for an aggregation equation, Comm. Partial Differential Equations 32 (12) (2007) 1941–1964.
[5] Andrea L. Bertozzi, Thomas Laurent, Jesús Rosado, Lp theory for the multidimensional aggregation equation, Comm. Pure Appl. Math. 64 (1) (2011) 45–83.
[6] José A. Carrillo, Marco DiFrancesco, Alessio Figalli, Thomas Laurent, Dejan Slepcev, Global-in-time weak measure solutions and finite-time aggregation for nonlocal interaction equations, Duke Math. J. 156 (2) (2011) 229–271.
[7] Andrew J. Bernoff, Chad M. Topaz, Nonlocal aggregation models: A primer of swarm equilibria, SIAM Rev. 55 (4) (2013) 709–747.
[8] Razvan C. Fetecau, Yanghong Huang, Theodore Kolokolnikov, Swarm dynamics and equilibria for a nonlocal aggregation model, Nonlinearity 24 (10) (2011) 2681.
[9] James H. Von Brecht, David Uminsky, Theodore Kolokolnikov, Andrea L. Bertozzi, Predicting pattern formation in particle interactions, Math. Models Methods Appl. Sci. 22 (2012) 1140002.
[10] Razvan C. Fetecau, Yanghong Huang, Equilibria of biological aggregations with nonlocal repulsive–attractive interactions, Physica D 260 (2013) 49–64.
[11] Andrew J. Leverentz, Chad M. Topaz, Andrew J. Bernoff, Asymptotic dynamics of attractive-repulsive swarms, SIAM J. Appl. Dyn. Syst. 8 (3) (2009) 880–908.
[12] José A. Carrillo, Katy Craig, Yao Yao, Aggregation-diffusion equations: dynamics, asymptotics, and singular limits, in: Active Particles, Vol. 2, Springer, 2019, pp. 65–108.
[13] Raluca Eftimie, Gerda de Vries, Mark A. Lewis, Complex spatial group patterns result from different animal communication mechanisms, Proc. Natl. Acad. Sci. 104 (17) (2007) 6974–6979.

[14] Michael te Vrugt, Hartmut Löwen, Raphael Wittkowski, Classical dynamical density functional theory: from fundamentals to applications, Adv. Phys. 69 (2) (2020) 121–247.
[15] Rinaldo M. Colombo, Magali Lécureux-Mercier, Nonlocal crowd dynamics models for several populations, Acta Math. Sci. 32 (1) (2012) 177–196.
[16] Bertram Düring, Peter Markowich, Jan-Frederik Pietschmann, Marie-Therese Wolfram, Boltzmann and Fokker–Planck equations modelling opinion formation in the presence of strong leaders, Proc. R. Soc. A: Math., Phys. Eng. Sci. 465 (2112) (2009) 3687–3708.
[17] Carlos Escudero, Fabricio Macia, Juan J.L. Velázquez, Two-species-coagulation approach to consensus by group level interactions, Phys. Rev. E 82 (1) (2010) 016113.
[18] Nancy Rodríguez, Lenya Ryzhik, Exploring the effects of social preference, economic disparity, and heterogeneous environments on segregation, Commun. Math. Sci. 14 (2) (2016) 363–387.
[19] Marco Di Francesco, Simone Fagioli, Measure solutions for non-local interaction pdes with two species, Nonlinearity 26 (10) (2013) 2777.
[20] Valeria Giunta, Thomas Hillen, Mark Lewis, Jonathan R. Potts, Local and global existence for nonlocal multispecies advection-diffusion models, SIAM J. Appl. Dyn. Syst. 21 (3) (2022) 1686–1708.
[21] Alan Mackey, Theodore Kolokolnikov, Andrea L. Bertozzi, Two-species particle aggregation and stability of co-dimension one solutions, Discrete Contin. Dyn. Syst. Ser. B 19 (5) (2014) 1411.
[22] Joep H.M. Evers, Razvan C. Fetecau, Theodore Kolokolnikov, Equilibria for an aggregation model with two species, SIAM J. Appl. Dyn. Syst. 16 (4) (2017) 2287–2338.
[23] José A. Carrillo, Yanghong Huang, Markus Schmidtchen, Zoology of a nonlocal cross-diffusion model for two species, SIAM J. Appl. Math. 78 (2) (2018) 1078–1104.
[24] Martin Burger, Marco Di Francesco, Simone Fagioli, Angela Stevens, Sorting phenomena in a mathematical model for two mutually attracting/repelling species, SIAM J. Math. Anal. 50 (3) (2018) 3210–3250.
[25] Julien Barre, Pierre Degond, Diane Peurichard, Ewelina Zatorska, Modelling pattern formation through differential repulsion, 2019, arXiv preprint arXiv:1906.00704.
[26] Martin Burger, Jan-Frederik Pietschmann, Helene Ranetbauer, Christian Schmeiser, Marie-Therese Wolfram, Mean field models for segregation dynamics, 2018, arXiv preprint arXiv:1808.04069.
[27] Marco Cicalese, L. De Luca, Matteo Novaga, Marcello Ponsiglione, Ground states of a two phase model with cross and self attractive interactions, SIAM J. Math. Anal. 48 (5) (2016) 3412–3443.
[28] J.W. Cahn, J.E. Hilliard, Free energy of a nonuniform system I. Interfacial free energy, J. Chem. Phys. 28 (1957) 258–267.
[29] Giambattista Giacomin, Joel L. Lebowitz, Phase segregation dynamics in particle systems with long range interactions II: Interface motion, SIAM J. Appl. Math. 58 (6) (1998) 1707–1729.
[30] Peter W. Bates, On some nonlocal evolution equations arising in materials science, Nonlinear Dyn. Evol. Equ. 48 (2006) 13–52.
[31] Robert L. Pego, Front migration in the nonlinear Cahn-Hilliard equation, Proc. R. Soc. Lond. Ser. A Math. Phys. Eng. Sci. 422 (1863) (1989) 261–278.
[32] William W. Mullins, Robert F. Sekerka, Morphological stability of a particle growing by diffusion or heat flow, J. Appl. Phys. 34 (2) (1963) 323–329.
[33] Peter W. Voorhees, The theory of ostwald ripening, J. Stat. Phys. 38 (1985) 231–252.
[34] Y. Nishiura, I. Ohnishi, Some mathematical aspects of the micro-phase separation of diblock copolymers, Physica D 84 (1995) 31–39.
[35] C.B. Muratov, Theory of domain patterns in systems with long-range interactions of Coulomb type, Phys. Rev. E 66 (6) (2002) 066108–+.
[36] Francesco Sciortino, Stefano Mossa, Emanuela Zaccarelli, Piero Tartaglia, Equilibrium cluster phases and low-density arrested disordered states: the role of short-range attraction and long-range repulsion, Phys. Rev. Lett. 93 (5) (2004) 055701.
[37] Rustum Choksi, Cyrill B. Muratov, Ihsan Topaloglu, An old problem resurfaces nonlocally: Gamow's liquid drops inspire today's research and applications, Notices Amer. Math. Soc. 64 (11) (2017) 1275–1283.
[38] Theodore Kolokolnikov, Hui Sun, David Uminsky, Andrea L. Bertozzi, A theory of complex patterns arising from 2D particle interactions, Phys. Rev. E, Rapid Commun. 84 (015, 203) (2011).
[39] Rustum Choksi, Razvan C. Fetecau, Ihsan Topaloglu, On minimizers of interaction functionals with competing attractive and repulsive potentials, in: Annales de l'Institut Henri Poincare (C) Non Linear Analysis, VOl. 32, Elsevier, 2015, pp. 1283–1305.
[40] Giovanni Alberti, Giovanni Bellettini, A nonlocal anisotropic model for phase transitions, Math. Ann. 310 (3) (1998) 527–560.
[41] Andrea Braides, et al., Gamma-Convergence for Beginners, Vol. 22, Clarendon Press, 2002.
[42] Giovanni Alberti, Giovanni Bellettini, A non-local anisotropic model for phase transitions: asymptotic behaviour of rescaled energies, European J. Appl. Math. 9 (3) (1998) 261–284.